THE IMA VOLUMES
IN MATHEMATICS
AND ITS APPLICATIONS VOLUME 29

James Glimm
Andrew J. Majda
Editors

Multidimensional Hyperbolic Problems and Computations

Springer-Verlag

James Glimm Andrew J. Majda
Editors

Multidimensional Hyperbolic Problems and Computations

With 86 Illustrations

Springer-Verlag
New York Berlin Heidelberg London
Paris Tokyo Hong Kong Barcelona

A NUMERICAL STUDY OF SHOCK WAVE REFRACTION AT A CO_2 / CH_4 INTERFACE†

ELBRIDGE GERRY PUCKETT‡

Abstract. This paper describes the numerical computation of a shock wave refracting at a gas interface. We study a plane shock in carbon dioxide striking a plane gas interface between the carbon dioxide and methane at angle of incidence α_i. The primary focus here is the structure of the wave system as a function of the angle of incidence for a fixed (weak) incident shock strength. The computational results agree well with the shock polar theory for regular refraction including accurately predicting the transition between a reflected expansion and a reflected shock. They also yield a detailed picture of the transition from regular to irregular refraction and the development of a precursor wave system. In particular, the computations indicate that for the specific case studied the precursor shock weakens to become a band of compression waves as the angle of incidence increases in the irregular regime.

Key words. shock wave refraction, conservative finite difference methods, Godunov methods, compressible Euler equations

AMS(MOS) subject classifications. 35L65, 65M50, 76L05

1. The Problem. In this work we consider a plane shock wave striking a plane gas interface at angle of incidence $0° < \alpha_i < 90°$. This is a predominantly two dimensional, inviscid phenomenon which we model using the two dimensional, compressible Euler equations with the incident shock wave and gas interface initially represented by straight lines.

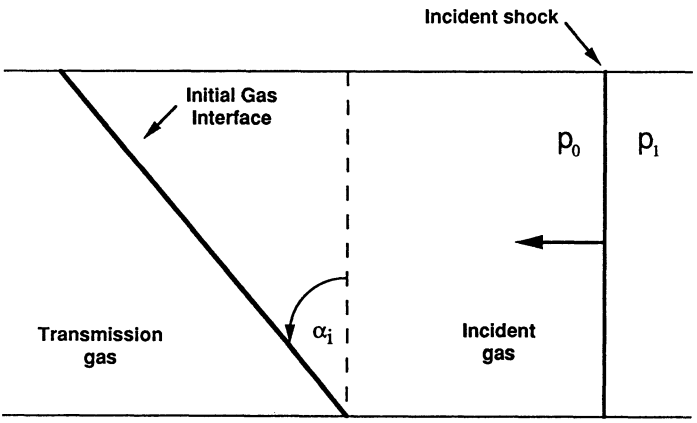

Figure 1 A diagram of the problem

†Work performed under the auspices of the U.S. Department of Energy at the Lawrence Livermore National Laboratory under contract number W-7405-ENG-48 and partially supported by the Applied Mathematical Sciences subprogram of the Office of Energy Research under contract number W-7405-Eng-48 and the Defense Nuclear Agency under IACRO 88-873.

‡Applied Mathematics Group, Lawrence Livermore National Laboratory, Livermore, CA 94550.

A diagram of the problem is shown in figure 1. The shock wave travels from right to left in the incident gas striking the interface from the right. This causes a shock wave to be transmitted into the transmission gas and a reflected wave to travel back into the incident gas. The reflected wave can either be a shock, an expansion, or a band of compression waves. Depending on the strength of the incident shock, the angle of incidence, and the densities and sound speeds of the two gases these three waves may appear in a variety of distinct configurations. In the simplest case the incident, transmitted, and reflected waves all meet at a single point on the interface and travel at the same speed along the interface. This is known as regular refraction. A diagram depicting regular refraction appears in figure 2.

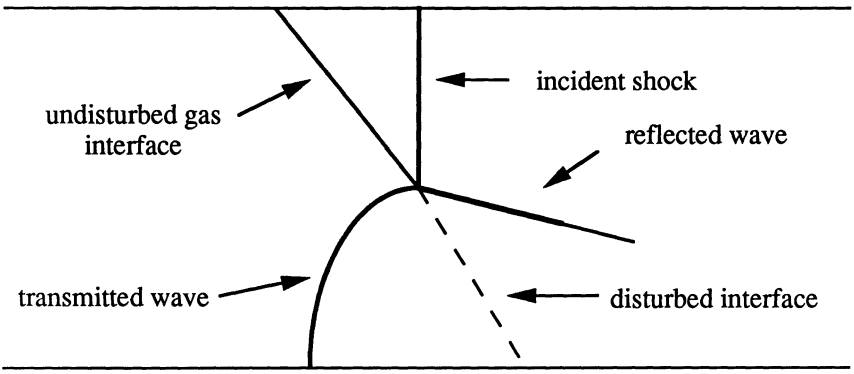

Figure 2 Regular Refraction

When the sound speed of the incident gas is less than that of the transmission gas the refraction is called *slow-fast*. In this case the transmitted wave can break away from the point of intersection with the incident and reflected waves and move ahead of them, forming what is known as a *precursor*. The incident shock can also form a stem between its intersection with the interface and its intersection with the reflected wave, similar to the well known phenomenon of Mach reflection. When the sound speed of the incident gas is greater than that of the transmission gas the refraction is called *fast-slow*. In this case the transmitted shock will lean back toward the interface. In this paper we restrict ourselves to the study of a specific sequence of slow-fast refractions. See Colella, Henderson, & Puckett [1] for a description of our work with fast-slow refraction.

For the purposes of modeling this phenomenon on a computer we assume the two gases are ideal and that each gas satisfies a γ-law equation of state,

$$p = A\rho^{\gamma}.$$

Here p is the pressure, ρ is the density, γ is the ratio of specific heats, and the coefficient A depends on the entropy but not on p and ρ. Note that γ is a constant for each gas but different gases will have different γ.

Given these assumptions the problem depends on the following four parameters: the angle of incidence α_i, the ratio of molecular weights for the two gases μ_i/μ_t,

the ratio of the γ for the two gases γ_i/γ_t, and the inverse incident shock strength $\xi_i = p_0/p_1$ where p_0 (*respectively* p_1) is the pressure on the upstream (*respectively* downstream) side of the shock. In this paper we consider the case when the incident gas is CO_2, the transmission gas is CH_4, the inverse incident shock strength is $\xi_i = 0.78$ and only the angle of incidence α_i is allowed to vary. Thus $\gamma_i = 1.288$, $\gamma_t = 1.303$, $\mu_i = 44.01$, $\mu_t = 16.04$, and the incident shock Mach number is 1.1182.

For this choice of parameters we find three distinct wave systems depending on α_i. These are: i) regular refraction with a reflected expansion, ii) regular refraction with a reflected shock, and iii) irregular refraction with a transmitted precursor. These wave systems appear successively, in the order listed, as α_i increases monotonically from head on incidence at $\alpha_i = 0°$ to glancing incidence at $\alpha_i = 90°$. In this paper we examine this sequence of wave patterns computationally much as one would design a series of shock tube experiments. This particular case has been extensively studied both experimentally and theoretically by Abd-el-Fattah & Henderson [2]. This has enabled us to compare our results with their laboratory experiments thereby providing us with a validation of the numerical method. See Colella, Henderson, & Puckett [1, 3] for a detailed comparison of our numerical results with the experiments of Abd-el-Fattah & Henderson. Once we have validated the numerical method in this manner we can use it to study the wave patterns in a detail heretofore impossible due to the limitations of schlieren photography and other experimental flow visualization techniques.

Early work on the theory of regular refraction was done by Taub [4] and Polachek & Seeger [5]. Subsequently Henderson [6] extended this work to irregular refractions, although a complete theory of irregular refraction still remains to be found. More recently, Henderson [7, 8] has generalized the definition of shock wave impedance given by Polachek & Seeger for the refraction of normal shocks.

Experiments with shock waves refracting in gases have been done by Jahn [9], Abd-el-Fattah, Henderson & Lozzi [10], and Abd-el-Fattah & Henderson [2, 11]. More recently, Reichenbach [12] has done experiments with shocks refracting at thermal layers and Haas & Sturtevant [13] have studied refraction by gaseous cylindrical and spherical inhomogeneities. Earlier, Dewey [14] reported on precursor shocks from large scale explosions in the atmosphere. Some multiphase experiments have also been done: Sommerfeld [15] has studied shocks refracting from pure air into air containing dust particles while Gvozdeava *et al.* [16] have experimented with shocks passing from air into a variety of foam plastics.

Some recent numerical work on shock wave refractions include Grove & Menikoff [17] who examined anomalous refraction at interfaces between air and water and Picone *et al.* [18] who studied the Haas & Sturtevant experiments at Air/He and Air/Freon cylindrical and spherical interfaces. Fry & Book [19] have considered refraction at heated layers while Glowacki *et al.* [20] have studied refraction at high speed sound layers and Sugimura, Tokita & Fujiwara [21] have examined refraction in a bubble-liquid system.

2. The Shock Polar Theory.

2.1 A Brief Introduction to the Theory. In this section we present a brief introduction to the theory of regular refraction. This theory is a straightforward extension of von Neumann's theory for regular reflection (von Neumann [22]) and is most easily understood in terms of shock polars. The theory is predicated on the observation that oblique shocks turn the flow. Consider a stationary oblique shock. If we call the angle by which the flow is turned δ (see figure 3), then δ is completely determined by the upstream state (ρ_0, p_0, u_0, v_0) and the shock strength p/p_0 where p denotes the post-shock pressure.

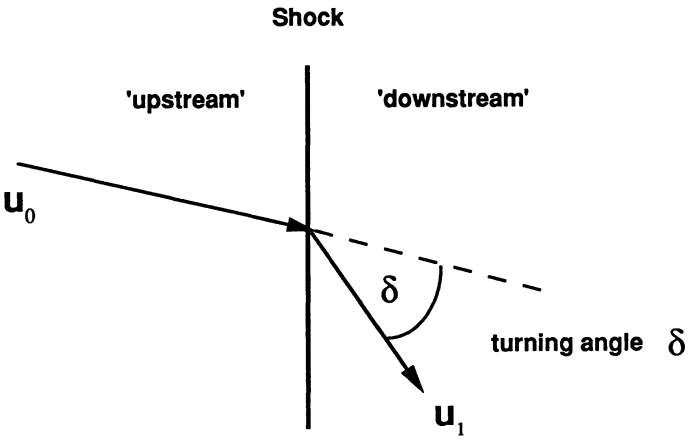

Figure 3 An oblique shock turns the flow velocity towards the shock

For a γ-law gas the equation governing this relation is

$$tan\,(\delta) = \frac{\left(\frac{p}{p_0} - 1\right)\sqrt{\frac{2\gamma M_S^2}{\gamma+1} - \frac{\gamma-1}{\gamma+1} - \frac{p}{p_0}}}{\left(1 + \gamma M_S^2 - \frac{p}{p_0}\right)\sqrt{\frac{\gamma-1}{\gamma+1} + \frac{p}{p_0}}} \tag{2.1}$$

where M_S is the freestream Mach number upstream of the shock (e.g. see Courant & Friedrichs [23]). If we now allow the shock strength to vary and plot $\log(p/p_0)$ versus the turning angle δ we obtain the graph shown in figure 4, commonly referred to as a *shock polar.*

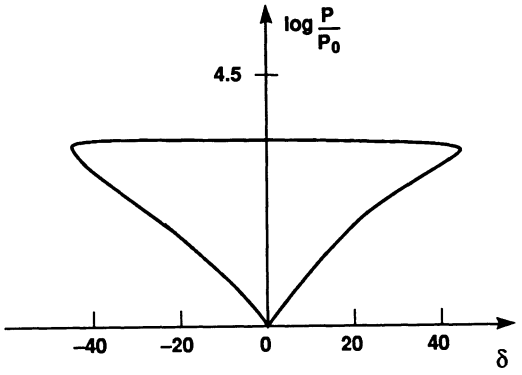

Figure 4 A Shock Polar

Recall that, by definition, in regular refraction the incident, transmitted, and reflected waves all meet at a single point on the interface. We now assume that these waves are locally straight lines in a neighborhood of this point and (for the moment) that the reflected wave is a shock. Each of these shocks will turn the flow by some amount, say δ_i, δ_t, and δ_r respectively (figure 5) and each of these angles will satisfy (2.1) with the appropriate choice of M_S, γ, and p/p_0.

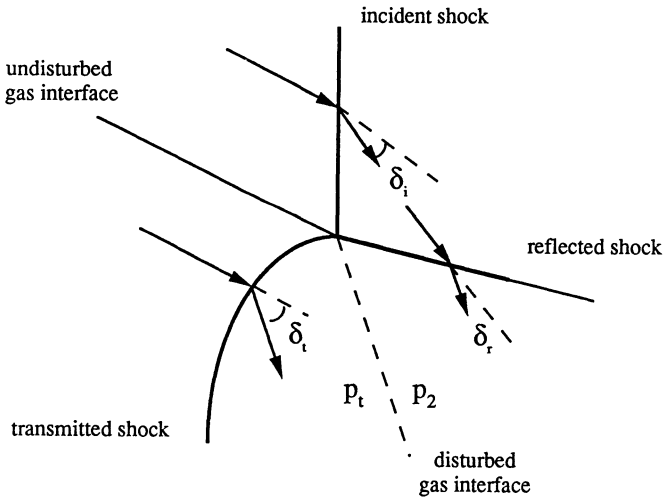

Figure 5 The shock polar theory for regular refraction is based on the fact that the flow must be parallel to the gas interface both above and below the intersection of the shocks. Thus, $\delta_t = \delta_i + \delta_r$. All shocks are assumed to be locally straight in a neighborhood of this intersection.

Furthermore, since the interface is a contact discontinuity we must have

$$p_t = p_2 \tag{2.2}$$

$$\delta_i + \delta_r = \delta_t \tag{2.3}$$

where the latter condition follows from the fact that the flow is parallel to the interface both upstream and downstream of the intersection of the incident, transmitted and reflected shocks. Note that the interface is, in general, deflected forward downstream of this intersection.

The problem now is as follows. Given the upstream state on both sides of the interface $(\rho_{0i}, p_0, u_{0i}, v_{0i})$ and $(\rho_{0t}, p_0, u_{0t}, v_{0t})$, the inverse incident shock strength ξ_i, and the angle of incidence α_i determine all other states. Let (ρ_1, p_1, u_1, v_1) denote the state downstream of the incident shock (upstream of the reflected shock) and let (ρ_t, p_t, u_t, v_t) and (ρ_2, p_2, u_2, v_2) denote the states downstream of the transmitted and reflected shocks respectively. For certain values of the given data this information is sufficient to completely determine all of the unknown states, although not necessarily uniquely. For example one can derive a 12th degree polynomial in the transmitted shock strength p_t/p_0 from (2.1-3), which for regular reflection has as one root the observed transmitted shock strength (Henderson [8]). The other roots either do not appear in laboratory experiments or are complex, and hence not physically meaningful. Note that knowledge of the transmitted shock strength p_t/p_0 is sufficient to determine all of the other states.

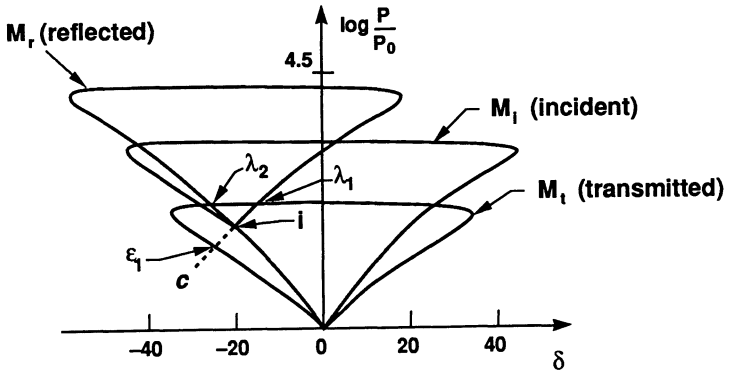

Figure 6 Each intersection of the transmitted shock polar and the reflected shock polar represents a possible wave configuration for regular refraction.

The physically meaningful roots of this polynomial may also be found by plotting the shock polars for the three waves in a common coordinate system. An example is shown in figure 6. Note that we have scaled the reflected shock strength p_2/p_1 by p_1/p_0 and translated δ_r by δ_i. Thus the plot of the reflected shock polar is given by $\log(p_2/p_0) = \log(p_2/p_1) + \log(p_1/p_0)$ versus $\delta_r + \delta_i$. This causes the base of

the reflected shock polar ($p_2 = p_1$) to coincide with the map of the incident shock on the incident shock polar (δ_i , p_1/p_0), labeled 'i' in the figure. In this shock polar diagram any intersection of the transmitted and reflected shock polars represents a physically meaningful solution to the problem, i.e. a pair of downstream states (ρ_t, p_t, u_t, v_t) and (ρ_2, p_2, u_2, v_2) such that all of the states satisfy the appropriate shock jump conditions and the boundary conditions (2.2-3). Note that more than one such intersection may exist. For example, in figure 6 there are two, labeled λ_1 and λ_2.

It is also the case that for some values of the initial data $(\rho_{0i}, p_0, u_{0i}, v_{0i})$, $(\rho_{0t}, p_0, u_{0t}, v_{0t})$, ξ_i and α_i, the transmitted and reflected shock polars do not intersect. It is interesting to inquire whether the existence of such an intersection exactly coincides with the occurrence of regular refraction in laboratory experiment. We will discuss this point further below.

We can extend the shock polar theory to include reflected waves which are centered expansions by adjoining to the reflected shock polar the appropriate rarefaction curve for values of $p_2 < p_1$. Let $q = \sqrt{u^2 + v^2}$ denote the magnitude of flow velocity, c the sound speed, and define the Mach angle μ by $\mu = \sin^{-1} 1/\mathrm{M}$ where $\mathrm{M} = q/c$ is the local Mach number of the flow. Then this rarefaction curve is given by

$$\delta = \pm \int_{p_1}^{p_2} \frac{\cos \mu}{qc\rho}\, dp \tag{2.4}$$

(see Grove [24]). This curve is sometimes referred to as a *rarefaction polar*. The sign will determine which branch of the shock polar is being extended. In figure 6 the branch corresponding to a negative turning angle δ_r has been plotted with a dotted line and labeled with a c. The intersection of this curve with the transmitted shock polar has been labeled ϵ_1. In some cases there may be two intersections. Each intersection represents a wave system in which the state (ρ_1, p_1, u_1, v_1) is connected to the state (ρ_2, p_2, u_2, v_2) across a centered rarefaction. Such systems are also found to occur in laboratory experiments (e.g. Abd-el-Fattah & Henderson [2]).

2.2 A Shock Polar Sequence. In this section we present the shock polar diagrams for the CO_2/CH_4 refraction with $\xi_i = 0.78$. The data was chosen as specified in Section 1 with only the angle α_i being allowed to vary. In figure 7 we present four shock polar diagrams. These correspond to the two types of regular refraction - namely regular refraction with a reflected expansion (RRE) and regular refraction with a reflected shock (RRR) - the transition between these two states, and the transition between regular and irregular refraction. The polars are labeled M_i, M_t, and M_r, which represent the freestream Mach numbers upstream of the incident, transmitted, and reflected waves respectively. To the right of each shock polar diagram is a small diagram of the wave system in which the initial interface is denoted by an m, and the deflected interface by a D.

In each of the shock polar diagrams the tops of the incident and reflected polars have not been plotted in order to allow us to focus on the intersections which are of interest. As stated above the map of the incident shock on the incident shock

polar is labeled i. This point corresponds to the base of the reflected shock polar. The intersection of the incident shock polar with the transmitted shock polar has been labeled A_1.

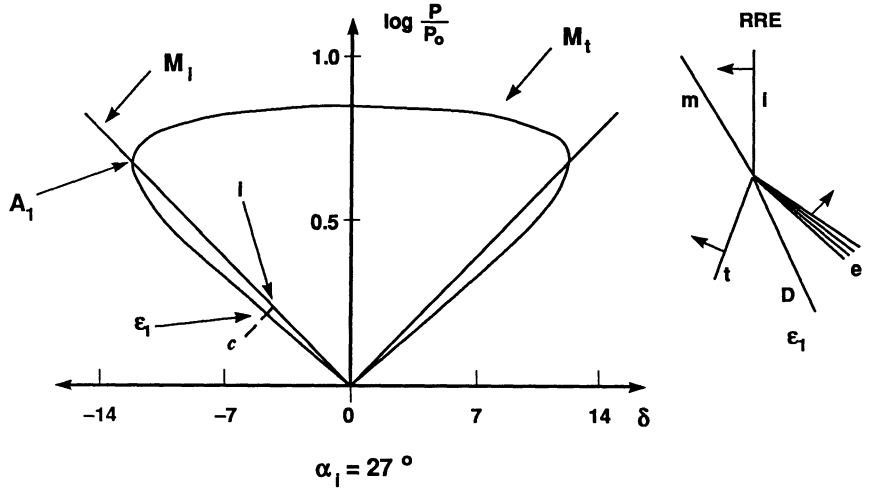

Figure 7a

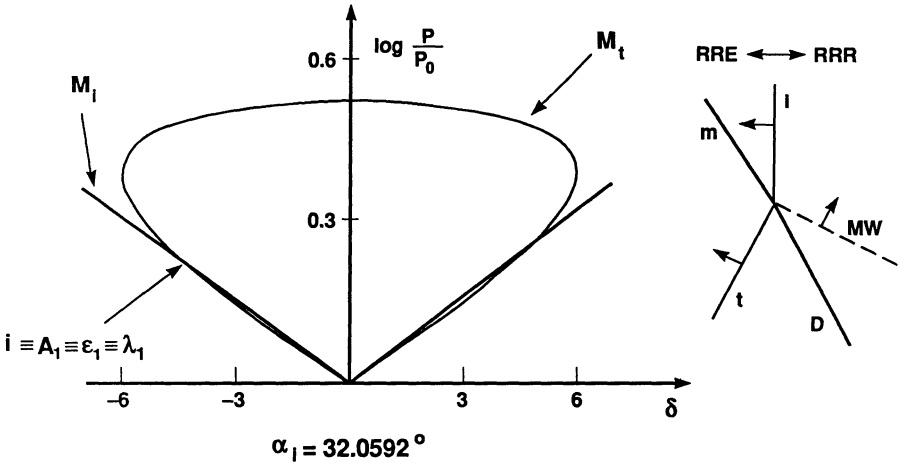

Figure 7b

In figure 7 a) we plot the polars for $\alpha_i = 27°$. Here we have only plotted the reflected rarefaction polar c and its intersection with the transmitted shock polar ϵ_1, not the reflected shock polar. There still exist two solutions λ_1 and λ_2 with a reflected shock but ϵ_1 is the solution observed in the laboratory (Henderson [2]). If we now continuously increase the angle α_i the points i and A_1 move towards each other until they coincide at $\alpha_i \approx 32.0592°$. Here there is no need for a reflected

shock or expansion since $\delta_i = \delta_t$. The shock polar diagram for this value of α_i appears in figure 7 b) with the polar for the reflected wave omitted. Note that this is a solution of the problem for which the pressure jump across the reflected wave is vanishingly small, i.e. it is a Mach wave (labeled MW in the small diagram on the right). This is the theoretical transition point between regular reflection with a reflected expansion and regular reflection with a reflected shock, RRE $\rightleftharpoons$ RRR, and at this point the solutions ϵ_1 and λ_1 coincide. At this point we have equality of the wave impedances and hence total transmission of the incident shock into the CH_4. (See Henderson [7, 8].)

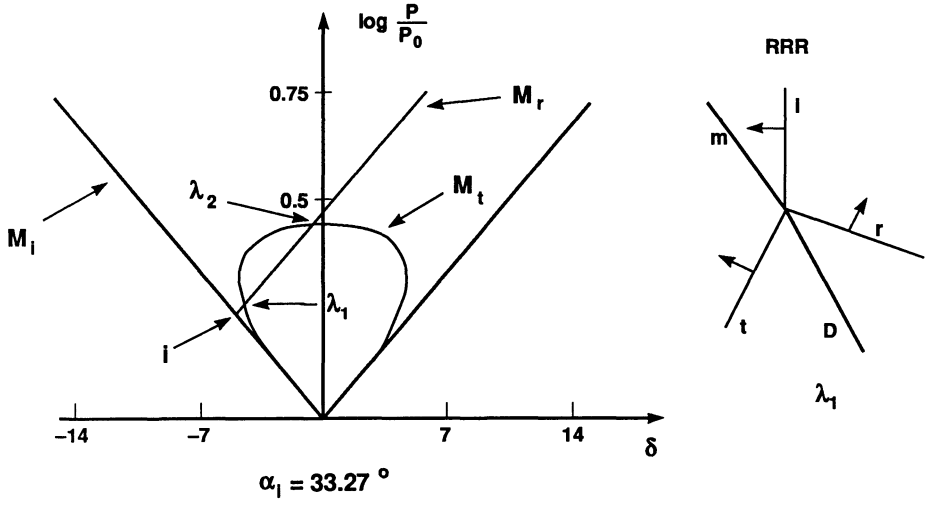

Figure 7c

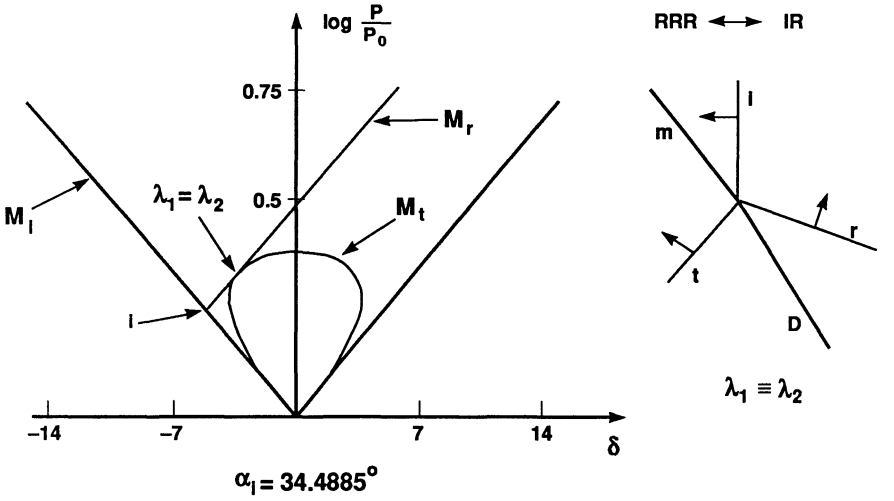

Figure 7d

Further increase in the angle α_i yields a situation in which the rarefaction curve no longer intersects the transmitted shock polar. However both solutions λ_1 and λ_2 corresponding to reflected shocks still exist. It is the weaker of these solutions, λ_1, which is observed in the laboratory (Henderson [2]). A diagram depicting RRR and the corresponding shock polars appears in figure 7 c). Further continuous increase in α_i results in the transmitted shock polar shrinking relative to the other two polars. This causes the solutions λ_1 and λ_2 to approach each other until they coincide at $\alpha_i \approx 34.4885°$ as shown in figure 7 d). Any further increase in α_i results in a situation where there is no longer an intersection of the reflected and transmitted polars. Thus $\lambda_1 = \lambda_2$ represents the point beyond which regular refraction is (theoretically) impossible. This is denoted RRR $\rightleftharpoons$ IR where IR stands for 'irregular refraction'. Other transition criteria have been proposed. For example, transition could occur when λ_1 coincides with the sonic point, i.e. the value of p_t/p_0 for which the flow speed behind the transmitted shock is sonic. Or transition could occur when λ_1 coincides with the value of p_t/p_0 for which δ_t achieves a maximum. In practice these points often lie so close to each other that it is next to impossible to determine which is the correct criterion from examining schlieren photographs or contour plots. We will discuss this point further after we present the results of our numerical computations in section 4 below.

3. The Numerical Method. We solve the Euler equations for two dimensional, compressible fluid flow. In conservation form these equations are

$$U_t + \nabla \cdot \mathbf{F}(U) = 0 \tag{3.1}$$

where

$$U = (\rho, \rho u, \rho v, \rho E)^T$$

and (u, v) is the velocity, E the total energy per unit mass, and $\mathbf{F} = (F, G)^T$ with

$$F = (\rho u, \rho u^2 + p, \rho uv, \rho uE + up)^T,$$

$$G = (\rho v, \rho uv, \rho v^2 + p, \rho vE + vp)^T.$$

We solve these equations on a rectangular mesh with grid spacing Δx and Δy and use absorbing boundary conditions on the right hand wall of the computational domain and reflecting boundary conditions on the other three walls.

The following four features of our numerical method are important to the accurate computation of the shock refraction problem.

1) A second order Godunov method for solving the fluid flow equations

2) A local, adaptive gridding strategy

3) A strategy for tracking the fluid interface based on the partial volumes of the fluid components in multifluid cells

4) An algorithm for accurately modeling the disparate thermodynamic properties of the two gases on a subgrid scale.

Currently we use an operator split version of the numerical method. In other words, we solve a succession of one dimensional problems at each time step, alternating the order of the x and y sweeps at alternate time steps. Effective unsplit techniques are available for solving equations (3.1) but our interface tracking algorithm requires operator splitting. We are currently developing an improved interface algorithm that will remove this restriction and we will report on it in a future work.

3.1 The Solution of the Euler equations. We use a second order Godunov method to solve the two dimensional compressible Euler equations. Since these methods have been widely discussed in the literature we refrain from going into detail here. Instead we refer the interested reader to van Leer [25], Colella & Woodward [26], and Colella & Glaz [27]. It should be remarked that in this work we use a piecewise linear approximation to the quantities in each grid cell rather than a piecewise parabolic approximation as discussed in Colella & Woodward [26].

3.2 Adaptive Mesh Refinement. In order to concentrate most of the computational work in regions of physical interest we employ a local adaptive gridding strategy called Adaptive Mesh Refinement (AMR) [28, 29, 30, 31, 32]. The basic idea behind AMR is to estimate the local truncation error at each cell center and tag those cells in which the error is unacceptably large. One then finds a collection of rectangles, all of which are contained in the original grid, in such a way that each of the tagged cells is contained in one of these rectangles. The optimum set of rectangles is determined by minimizing a cost function. So, for example, one large rectangle may be chosen instead of two smaller rectangles with fewer untagged grid points because the large rectangle leads to more optimal vector lengths on a Cray computer. This cost function also takes into account the overhead associated with setting up the boundary conditions for each fine grid.

Each of the new rectangles is then subdivided into smaller cells $1/k$th the size of the original coarse cell (generally $k = 2$ or 4) and the values of the state variables are assigned to each of the new cells in such a way as to conserve all of the appropriate quantities. The equations of motion are then solved on the finer mesh with boundary values obtained from adjacent grids of the same level of refinement or interpolated from the coarser mesh. Note that in order for the CFL condition to be satisfied one must take k times as many time steps on the finer grid, each $1/k$th the size of the coarse grid time step. The value of the state variables in a coarse grid cell which contains fine grid cells is set to the average of the values in the fine grid cells. In order to guarantee conservation at grid boundaries care is taken so that if the boundary of a fine grid abuts a coarse grid (and not another fine grid), then the flux across each coarse cell wall is equal to the sum of the fluxes out of each fine cell which abuts that coarse cell. This adaptive gridding procedure can be recursively extended to obtain multiple levels of refinement.

In figure 8 we show a diagram of a shock wave refraction computation which has been refined in certain important regions. For further details regarding our implementation of the AMR algorithm the reader is referred to Berger & Colella [32].

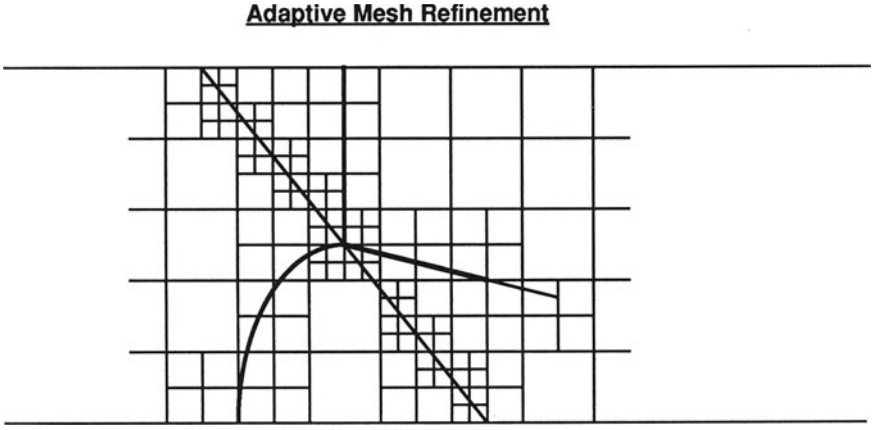

Figure 8 This is how the adaptive gridding algorithm might grid the wave system in figure 2 with two levels or refinement.

3.3 Tracking the Gas Interface.

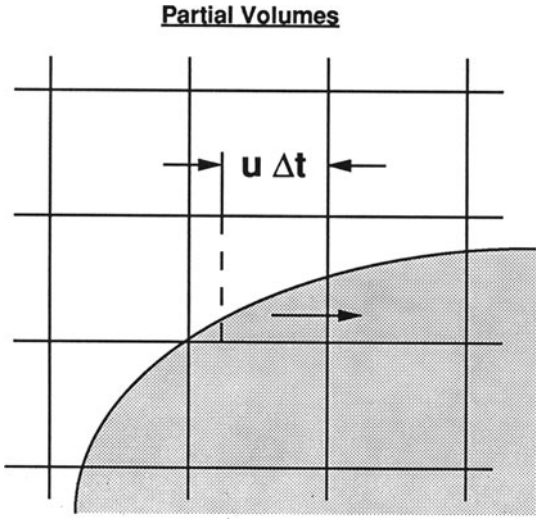

Figure 9 The fraction of dark fluid to the right of the dotted line is advected into the neighboring cell on the right. In this example u is positive.

We employ a partial volumes based approach to the problem of tracking the gas interface. Figure 9 depicts a portion of an interface and its intersection with several grid cells. At the start of the computation in each cell we calculate the ratio f_{ij} of volume occupied by the dark fluid to the total volume of the cell. So $0 \leq f_{ij} \leq 1$ for all cells with $f_{ij} = 0$ if the cell contains all light fluid and $f_{ij} = 1$ if the cell

contains all dark fluid. The interface is then advanced in time as follows. At each time step,

1) Given the partial volumes f_{ij} we create an approximation to the interface in each multifluid cell ($0 < f_{ij} < 1$), such that this approximate interface divides the cell into the correct ratio of fluid volumes.

2) For the x-sweep we divide the cell by a vertical line into two rectangles with areas $|u|\Delta t\Delta y$ and $(\Delta x - |u|\Delta t)\Delta y$. We then move that portion of the dark fluid which lies inside the rectangle on the right (if $u > 0$ and on the left if $u < 0$) into the adjacent cell to the right (if $u > 0$ and left if $u < 0$). A cartoon depicting an example of this procedure when $u > 0$ is shown in figure 9. An identical procedure is performed for the y-sweep with u replaced by v, Δy replaced by Δx, etc.

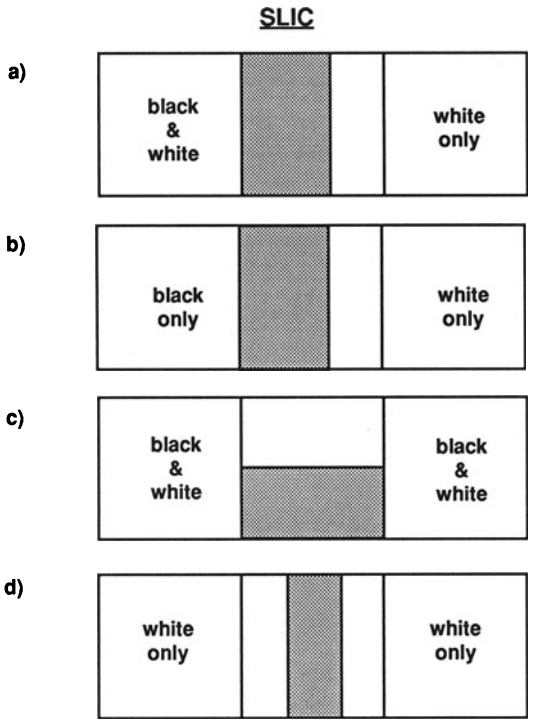

Figure 10 Given the states in the adjacent cells this is how SLIC will draw the interface for a pass in the x-direction. There are five other cases obtained by interchanging black and white and/or left and right.

It remains for us to specify how one recreates the interface given the partial volumes f_{ij}. Here we employ the SLIC (Simple Line Interface Calculation) algorithm created by Noh and Woodward [33]. In determining the interface in the i,jth cell for an x-sweep SLIC considers only the ratio f_{ij} in that cell and the presence

or absence of light and dark fluids in the two adjoining (in the x-direction) cells. Figure 10 depicts how the interface is drawn in four of the nine possible cases. The other five cases can be found by reversing the roles of the light and dark fluids and/or by reversing left and right. Figure 11 contains an example of how the SLIC algorithm would reconstruct the interface in figure 9 for a sweep in the x-direction. The interface is reconstructed in an analogous manner for a sweep in the y-direction.

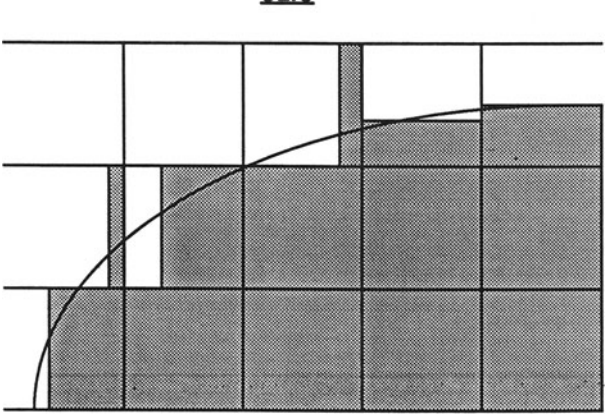

Figure 11 This is how SLIC would recreate the interface in figure 9 for a sweep in the x-direction.

It should be emphasized that the only feature of the flow which we are tracking is the actual gas interface. All of the shocks and other discontinuities in the flow are *captured* by the underlying numerical solution of the equations of gas dynamics.

3.4 Subgrid Modeling of the Multifluid Components. We employ a recent innovation for modeling the thermodynamic properties of distinct fluid components which occupy the same grid cell. The principle goal of this algorithm is to ensure that fluid components of different densities will undergo the correct relative compressions or expansions when the cell they occupy is subjected to pressure forces. This algorithm is based on the assumption that the various fluid components in each cell are in pressure equilibrium with one another and that each cell has a single velocity. From a physical point of view the assumption of pressure equilibrium is not unreasonable since pressure is continuous across a contact discontinuity. The requirement that the cell have a single velocity is not appropriate in more than one dimension since slip will be generated at a fluid interface. Thus we track the jump in thermodynamic variables across the interface, while capturing the jump in tangential velocity using the underlying conservative finite difference method. This algorithm is applicable to any number of fluid components. We refer the reader to Colella, Glaz & Ferguson [34] for a detailed description of this algorithm.

4. The Computational Results. We used the computational method described above to model a weak shock ($\xi_i = 0.78$) in CO_2 striking an plane interface

with CH_4. In this context the word 'weak' means that the flow downstream of the incident shock remains supersonic and hence it is possible for the reflected wave to be a shock. We remark that Abd-el-Fattah & Henderson [2] (who refer to the case with $\xi_i = 0.78$ as being a 'very weak' incident shock) examined the effect changing the incident shock strength has on the structure of these wave systems.

In figure 12 we reproduce contour plots of log p for a sequence of α_i with $27° \leq \alpha_i \leq 65°$. Next to each contour plot we show an enlargement of the intersection of the incident, transmitted, and reflected waves with the gas interface. In each of these contour plots there is a straight line running diagonally from upper left to lower right. This line represents the initial gas interface before being struck by the shock. It is simply a line drawn for easy reference and is *not* a contour of log p.

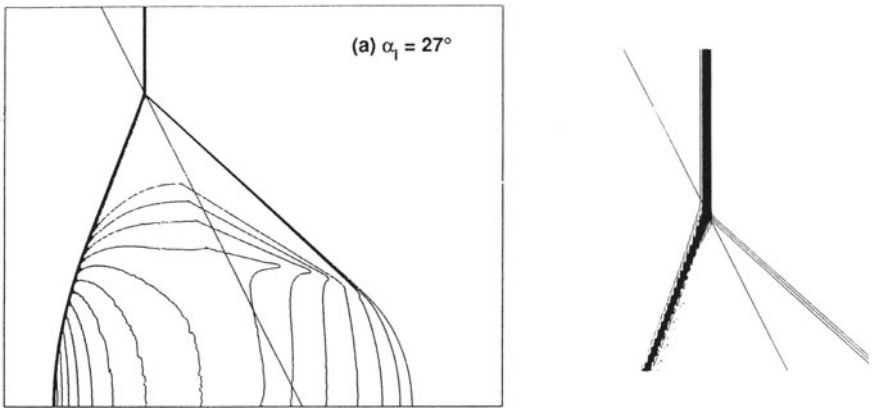

Figure 12a

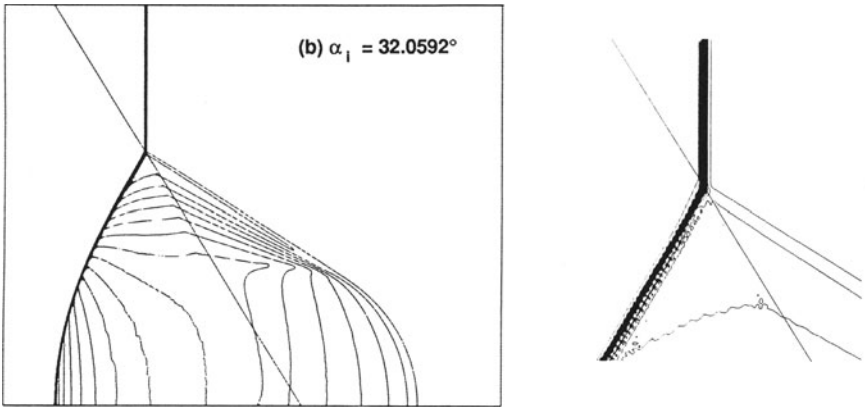

Figure 12b

In figure 12 a) $\alpha_i = 27°$ and the resulting wave system is a regular reflection with a reflected expansion corresponding to figure 7 a). In figure 12 b) we have

increased α_i to 32.0592°. This is the theoretical boundary between a reflected expansion and a reflected shock and corresponds to figure 7 b). It is apparent from the enlargement in figure 12 b) that the reflected wave is very nearly a Mach wave. This can be seen by noting that the reflected wave consists of two contours. The first is a continuation of the last contour in the incident shock and hence we know that the pressure decreases as we move across it from the state (ρ_1, p_1, u_1, v_1) towards the state (ρ_2, p_2, u_2, v_2). Similarly, since the second contour is a continuation of the last contour in the transmitted shock, the pressure must rise again as we cross it. The plotting program plots values of the pressure at fixed increments and hence the pressure value must be the same on these two contours. In other words, if these two contours were coincident then we would have a Mach wave. The discrepancy between figure 12 b) and an actual Mach wave is well within the range of acceptable numerical error given the level of refinement of the computation.

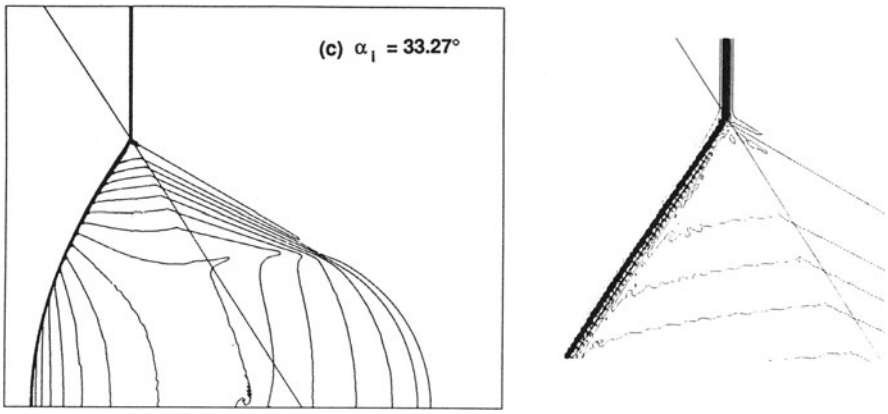

Figure 12c

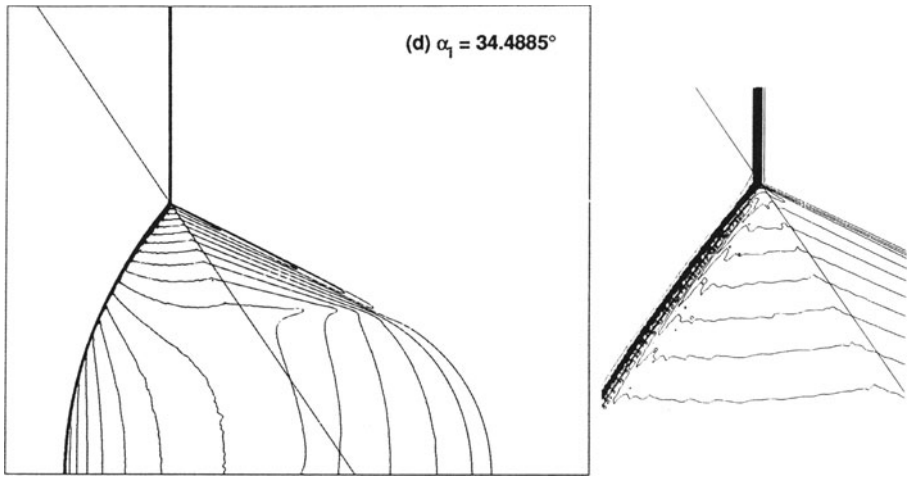

Figure 12d

If we increase α_i to 33.27° we find that the reflected wave has now become a shock. The contour plot appears in figure 12 c) and corresponds to the solution λ_1 shown in figure 7 c). Figure 12 d) contains the contour plot of log p for α_i = 34.4885°. This is the case $\lambda_1 = \lambda_2$ shown in figure 7d) and is the theoretical limit of regular refraction. Note that as α_i increases from 27° to 34.4885° the pressure contours emanating from the transmitted shock swing around until they are parallel and nearly coincident with the reflected shock. The relation (if any) of this phenomenon to the onset of irregular refraction and/or a precursor wave system remains to be investigated.

Figures 12 e) - h) contain a sequence of contours for α_i in the range beyond the theoretical limit of regular refraction. In figure 12 e) $\alpha_i = 38°$ which is several degrees beyond the theoretical limit of regular refraction. However it is very difficult to determine from the contour plot if this is still a regular refraction or not. This is a problem confronting anyone who attempts to interpret either numerical or experimental results in the region close to the transition. Similar problems are encountered when one attempts to determine the proper transition criterion for shock reflection. We remark that for the shock reflection problem it has been observed that for certain incident shock strengths regular reflection persists beyond the theoretical limit. See Colella & Henderson [35] for further details.

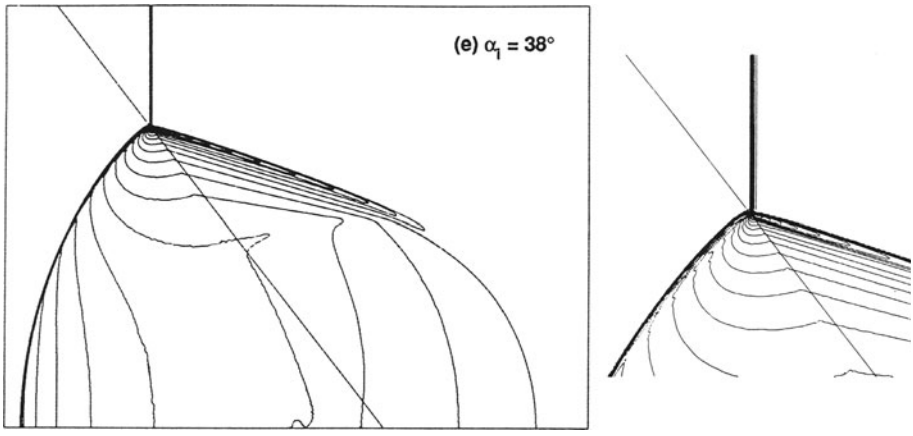

Figure 12e

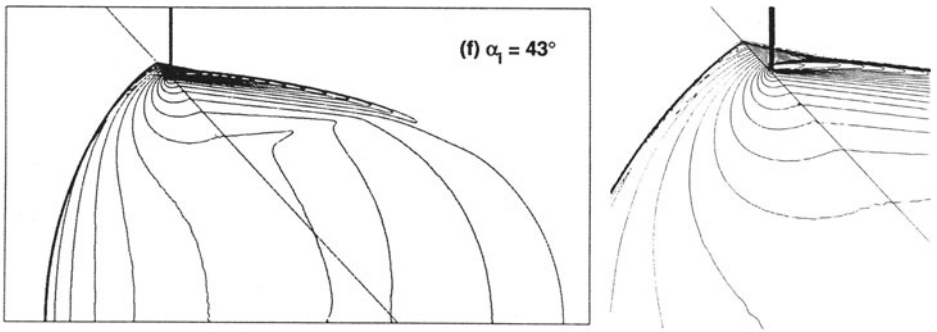

Figure 12f

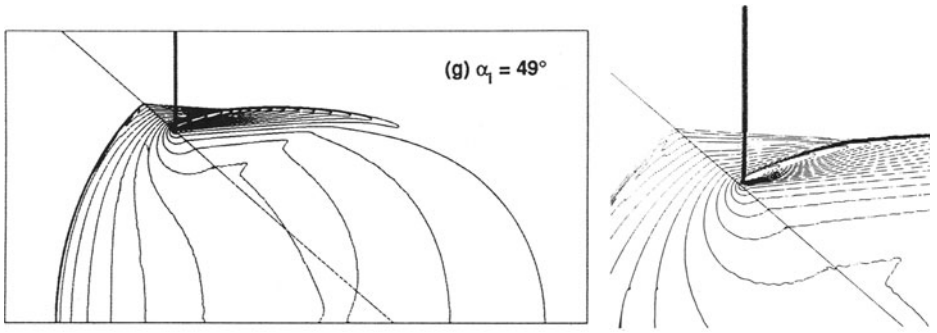

Figure 12g

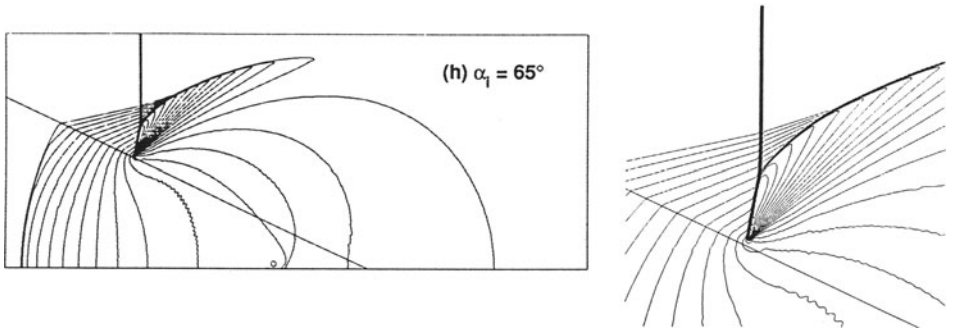

Figure 12h

By the time $\alpha_i = 43°$ in figure 12 f) it is clear that the transmitted shock has moved ahead of the incident shock and formed a precursor. Note that the precursor itself refracts back into the incident gas producing a small 'side shock' which interacts with the bottom of the incident shock. There is some indication from the enlargement that near the interface the precursor and side shocks are beginning to break up into a band of compression waves. In figures 12 g) & h)

this effect is much more pronounced. Based on schlieren photographs of shock tube experiments it had previously been thought that the transmitted and side waves remained shocks for all values of α_i in this range.

6. Conclusions. We have used a second order conservative finite difference method for solving the 2d compressible Euler equations to model the refraction of a weak shock at a CO_2/CH_4 interface. We modeled the gas interface with a simple interface tracking algorithm based on volume fractions. A new feature of this method is that the thermodynamic properties of distinct fluid components sharing a common multifluid cell are modeled separately. This allows components with disparate thermodynamic properties to undergo the appropriate expansions or compressions on a subgrid scale. We computed a sequence of refractions with fixed incident shock strength, varying only the angle of incidence α_i. For values of this angle lying in the theoretical range of regular refraction the computational results were in complete agreement with the shock polar theory. For values of α_i outside this range the contour plots reveal a detailed picture of the development of an irregular wave system with a precursor shock in the CH_4. Furthermore our results indicate that for the larger values of α_i in the irregular range the precursor degenerates into a band of compression waves. This is a new observation based on the greater detail available from the computational results as compared to earlier schlieren photographs.

Acknowledgements. The author would like to graciously acknowledge many fruitful discussions with Phil Colella and Roy Henderson.

REFERENCES

[1] P. Colella, L. F. Henderson and E. G. Puckett, *A Numerical Study of Shock Wave Refractions at a Gas Interface*, Proceedings of the AIAA 9th Computational Fluid Dynamics Conference (June 13-15,1989), pp. 426–439, Buffalo, New York.

[2] A. M. Abd-el-Fattah and L. F. Henderson, *Shock waves at a slow-fast gas interface*, J. Fluid Mech., 89 (1978), pp. 79–95.

[3] L. F. Henderson, P. Colella, and E. G. Puckett, *On the refraction of shock waves at a slow-fast gas interface*, submitted to the Journal of Fluid Mechanics.

[4] A. H. Taub, *Refraction of Plane Shock Waves*, Phys. Rev., 72 (1947), pp. 51–60.

[5] H. Polachek and R. J. Seeger, *On Shock Wave Phenomenon: Refraction of Shock Waves at a Gaseous Interface*, Phys. Rev., 84 (1951), pp. 922–929.

[6] L. F. Henderson, *The refraction of a plane shock wave at a gas interface*, J. Fluid Mech., 26 (1966), pp. 607–637.

[7] L. F. Henderson, *On shock impedance*, J. Fluid Mech., 40 (1970), pp. 719–735.

[8] L. F. Henderson, *On the refraction of shock waves*, J. Fluid Mech., 198 (1989), pp. 365–386.

[9] R. G. Jahn, *The refraction of shock waves at a gaseous interface*, J. Fluid Mech., 1 (1956), pp. 457–489.

[10] A. M. Abd-el-Fattah, L. F. Henderson and A. Lozzi, *Precursor shock waves at a slow-fast gas interface*, J. Fluid Mech., 76 (1976), pp. 157–176.

[11] A. M. Abd-el-Fattah and L. F. Henderson, *Shock waves at a fast-slow gas interface*, J. Fluid Mech., 86 (1978), pp. 15–32.

[12] H. Reichenbach, *Roughness and heated layer effects on shock wave propagation and reflection-experimental results*, E-Mach Inst. Rep. E24/85, Frieberg: Fraunhofer-Gesellschaft.

[13] J.-F. Haas and B. Sturtevant, *Interaction of weak shock waves with cylindrical and spherical gas inhomogeneities*, J. Fluid Mech., 181 (1987), pp. 41–76.

[14] J. M. Dewey, *Precursor Shocks Produced by a Large Yield Chemical Explosion*, Nature, 205 (1965), pp. 1306 only.

[15] M. Sommerfeld, *The unsteadiness of shock waves propagating through gas-particle mixtures*, Experiments in Fluids, 3 (1985), pp. 197–206.

[16] L. G. Gvozdeava, X. Faresov, M. Yu, J. Brossard, and N. Charpentier, *Normal shock wave reflexion on porous compressible material*, Prog. Astron. Aeron., 106 (1986), pp. 155-165.

[17] J. W. Grove and R. W. Menikoff, *Anomalous Refraction of a Shock Wave at a Fluid Interface*, Los Alamos Report LA-UR-89-778.

[18] J. M. Picone, J. P. Boris, E. S. Oran, and R. Ahearne, *Rotational Motion Generated by Shock Propagation Through a Nonuniform Gas*, in Proc. 15th Intl. Symp. on Shock Waves and Shock Tubes, ed. D. Bershader and R. Hanson, Stanford University Press.

[19] M. A. Fry and D. L. Book, *Shock Dynamics in Heated Layers*, in Proc. 15th Intl. Symp. on Shock Waves and Shock Tubes, ed. D. Bershader and R. Hanson, Stanford University Press.

[20] W. J. Glowacki, A. L. Kuhl, H. M. Glaz, and R. E. Ferguson, *Shock Wave Interaction with High Speed Sound Layers*, in Proc. 15th Intl. Symp. on Shock Waves and Shock Tubes, ed. D. Bershader and R. Hanson, Stanford University Press.

[21] T. Sugimura, K. Tokita, and T. Fujiwara, *Nonsteady Shock Wave Propagating in a Bubble-Liquid System*, AIAA J., 94 (1984), pp. 320-331.

[22] J. von Neumann, *Oblique Reflection of Shocks*, in Collected Works 6, ed. A. H. Taub Pergamon Press, New York (1963), pp. 238–299.

[23] R. Courant and K. O. Friedrichs, *Supersonic Flow and Shock Waves*, Springer Verlag, New York, 1976.

[24] J. Grove, *The Interaction of Shock Waves with Fluid Interfaces*, Advances in Applied Mathematics, 10 (1989), pp. 201–227.

[25] B. van Leer, *Towards the ultimate conservative difference scheme, a second order sequel to Godunov methods*, J. Comp. Phys., 32 (1979), pp. 101–136.

[26] P. Colella and P. Woodward, *The piecewise parabolic method (PPM) for gas dynamical simulations*, J. Comp. Phys., 54 (1984), pp. 174–201.

[27] P. Colella and H. M. Glaz, *Efficient solution algorithms for the Riemann problem for real gases*, J. Comp. Phys., 59 (1985), pp. 264–289.

[28] M. J. Berger and J. Oliger, *Adaptive mesh refinement for hyperbolic partial differential equations*, J. Comp. Phys., 53 (1984), pp. 482-512.

[29] M. J. Berger and A. Jameson, *Automatic adaptive grid refinement for the Euler equations*, AIAA J., 23 (1985), pp. 561–568.

[30] M. J. Berger, *Data structures for adaptive grid generation*, SIAM J. Sci. Stat. Comp., 7 (1986), pp. 904–916.

[31] M. J. Berger, *On conservation at grid interfaces*, SIAM J. Num. Anal. (1987).

[32] M. J. Berger and P. Colella, *Local adaptive mesh refinement for shock hydrodynamics*, J. Comp. Phys., 82 (1989), pp. 64–84.

[33] W. F. Noh and P. Woodward, *SLIC (Simple Line Interface Calculation)*, UCRL preprint 97196, Lawrence Livermore National Laboratory.

[34] P. Colella, H. M. Glaz, and R. E. Ferguson, *Multifluid algorithms for Eulerian finite difference methods*, manuscript.

[35] P. Colella and L. F. Henderson, *The von Neumann paradox for the diffraction of weak shock waves*, J. Fluid Mech. (to appear).